Mechanical Evolution of Solid Electrolyte Interphase on Metallic Lithium Studied by in situ Atomic Force Microscopy

Journal of The Electrochemical Society, 2023 **170** 010534

Mechanical Evolution of Solid Electrolyte Interphase on Metallic Lithium Studied by in situ Atomic Force Microscopy

Beatrice Wolff[1,2] **and Florian Hausen**[1,2,z]

[1]*Forschungszentrum Jülich GmbH, Institute of Energy and Climate Research, IEK-9, 52425 Jülich, Germany*
[2]*RWTH Aachen University, Institute of Physical Chemistry, 52074 Aachen, Germany*

Metallic lithium is a promising candidate as anode material in lithium batteries due to its high specific capacity and cell voltage. However, the high reactivity of metallic lithium leads to a rapid formation of the solid electrolyte interphase (SEI), even without an applied voltage. Unfortunately, the formation mechanism of the SEI is not yet fully understood. An exact understanding of the SEI includes mechanical properties, such as stiffness. Here, the mechanical properties during SEI formation are studied in an electrolyte consisting of 1.2 M $LiPF_6$ in a mixture of ethylene carbonate (EC) and ethyl methyl carbonate (EMC) without applied potential using in situ atomic force microscopy (AFM). The formation of the SEI is investigated by mapping the mechanical evolution of the surface. Thereby, changes of surface composition are visualised over time. Moreover, for the addition of vinylene carbonate as an additive to the electrolyte, the impact on the morphology as well as the stiffness is demonstrated.
 [DOI: 10.1149/1945-7111/acb01e]

Manuscript submitted November 2, 2022; revised manuscript received December 16, 2022. Published January 25, 2023. *This paper is part of the JES Focus Issue on Selected Papers from IMLB 2022.*

In recent years, lithium metal has become an increasingly interesting material for lithium battery anodes. An advantage in addition to a high specific capacity of 3860 mA h g^{-1} is its cell potential of −3.040 V versus the standard hydrogen electrode (SHE).[1–5] However, the use of metallic lithium remains currently challenging due to its reactive nature. Dendrite formation, eventually leading to short-circuit and thus limited lifetime,[6] as well as immediate formation of a solid electrolyte interphase (SEI)[7] upon contact with the electrolyte without any applied potential are currently the main aspects that require an exact understanding at sufficiently small scales.[8] Established formation cycles are not applicable in the case of metallic lithium as in contrast to typically used graphite electrodes the SEI already forms at more cathodic potentials than 1.4 V vs Li/Li^+.[9] Advantageous properties of the SEI combine high ionic conductivities and mechanical stability. For graphite based electrodes, the use of additives has been demonstrated in numerous studies to influence the SEI formation, thus proving a great step toward achieving better cell performance.[10–17] The influence of electrolyte additives for lithium metal anodes has been studied less.[18–21] Very recently, Weber et al. investigated the influence of the additive vinylene carbonate (VC) on the SEI formation on lithium metal in the electrolyte $LiPF_6$ in EC/EMC.[20] Employing scanning electrochemical microscopy (SECM) and gas chromotography-mass spectroscopy (GC-MS), the authors showed that the additive greatly decreases layer growth by passivation while the reaction with lithium in the same electrolyte but without additive continues over at least 19 days. Xu et al. studied the SEI formed on electrodeposited lithium by cryogenic transmission electron microscopy imaging (cryo-TEM), energy dispersive X-ray spectroscopy (EDS) and electron energy loss spectroscopy (EELS).[21] They demonstrated that the SEI in VC containing electrolyte exhibits a mosaic-like structure. While this structure isbased on organic species, Li_2O and Li_2CO_3, the SEI formed in the electrolyte without VC exhibits a multilayer structure consisting mainly of Li_2O. Apparently, all aforementioned components of the SEI show distinct mechanical properties, as also demonstrated on graphite surfaces by Shin et al.[22] Furthermore, Shen et al. provide evidence that the mechanical strength of the entire SEI strongly influences the growth of dendrites upon lithium deposition.[23] In this work, in situ atomic force microscopy is employed to investigate the formation of the SEI layer without applied potential and the temporal evolution of its mechanical properties within the first hours in an electrolyte composed of 1.2 M $LiPF_6$, ethylene carbonate (EC) and ethyl methyl carbonate (EMC). Additionally, the influence of the additive vinylene carbonate (VC) is assessed.

AFM allows for in situ observation of the sample surface on the nanoscale and has been pioneered by Aurbach et al. to study lithium metal surfaces in electrolytes.[24,25] Moreover, investigations of morphology combined with mechanical properties have been demonstrated on graphite[26] and silicon[27,28] anode materials. The aim of this work is to study the temporal evolution of the mechanical properties and the morphology of the SEI by in situ atomic force microscopy.

Experimental

Lithium foil was used as received in a thickness of 0.3 mm (Honjo Metal Co.,Ltd., Japan). No surface treatment was performed to ensure application related conditions. As electrolyte, either 1.2 M $LiPF_6$ dissolved in EC:EMC (3:7 by weight) or 1.2 M $LiPF_6$ dissolved in EC:EMC (3:7 by weight) + 5 wt% VC (Tomiyama, Japan) were used. These two electrolyte compositions will be referred to as EC/EMC and EC/EMC + VC.

For the in situ AFM experiments, lithium foil was fixed in an electrochemical AFM cell (Bruker, General purpose EC cell). Reference and counter electrodes were prepared by wrapping lithium foil around a piece of partly insulated copper wire. Experiments were conducted under open circuit voltage (OCV), no external potential was applied. The cell potential was tracked by a potentiostat (Biologic, SP300) and no variations were observed during the experiments.

AFM measurements were carried out inside a glove box filled with Argon ($O_2 < 0.1$ ppm, $H_2O < 0.1$ ppm, MBraun). All images of mechanical properties were obtained in PeakForce tapping quantitative nanomechanical mapping (QNM) mode (Bruker, proprietary mode).[29] An AFM tip made from boron doped diamond (ADAMA, AD-40-AS) was used to avoid artifacts from interactions between lithium foil and tip material. Calibration as well as determination of the individual tip radius were carried out using highly oriented pyrolytic graphite (HOPG) and a polystyrene film as reference samples, provided by Bruker. The stiffness was determined using the Derjaguin-Muller-Toporov (DMT) model.[30] The DMT model was fit in the contact regime of the force distance curves within the boundaries of 30%–90% of the range between maximum and minimum force.

AFM images were obtained continuously at the same sample spot over a period of three to six hours. These experiments were performed with the two aforementioned electrolytes and repeated multiple times.

[z]E-mail: f.hausen@fz-juelich.de

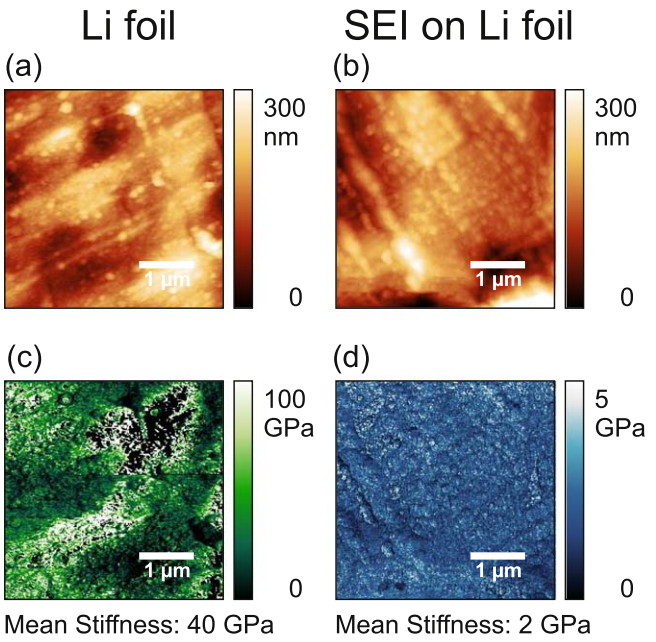

Figure 1. Topography a, b and corresponding Stiffness c, d of lithium foil a, c and the SEI layer after addition of the electrolyte EC/EMC b, d.

Care must be taken at least in this system when analysing peak force data files for "invalid" data points. These occur when the fit of the DMT model to the force distance curves results in non-meaningful values. As this phenomenon was partially observed for the system studied in this work, it is important to evaluate the individual force distance curves captured in the "peakforce capture files" in addition to the stiffness maps generated online during measurements.

Kelvin probe force microscopy (KPFM) was performed on the same instrument in PeakForce KPFM mode. A cantilever with a boron-doped diamond tip (ADAMA, AD-2.8-AS) was used.

Results

The evolution of topography and local stiffness of the SEI layer formed on metallic lithium foil without applied potential has been studied in situ as a function of time, when adding EC/EMC and EC/EMC + VC electrolytes to metallic lithium foil. The topography and stiffness of metallic lithium before and after adding the electrolyte is depicted in Fig. 1. Figure 1a displays the topography of a certain area of lithium foil. The surface exhibits several features: it is rather heterogenous and has line-shaped ridges which reflect the rolling process of the foil. Additionally, small particles of different sizes are present on the surface. The topography of the SEI layer that forms on the lithium surface after adding the electrolyte EC/EMC is shown in Fig. 1b. Here, the surface topography exhibits similar features. The stiffness maps corresponding to the aforementioned topographic images are presented in Figs. 1c and 1d for the lithium surface and the immediately formed SEI layer, respectively. The stiffness of the lithium surface illustrated in Fig. 1c shows a heterogeneous distribution. Values vary in a range of 100 GPa with a mean value of 40 GPa. The stiffness of the SEI layer depicted in Fig. 1d, however, exhibits much smaller values in a range of up to 5 GPa, with a mean value of 2 GPa. This reveals that the SEI layer is much softer than the lithium surface.

Figure 2 shows three typical images of the topography of different data sets obtained in the electrolyte EC/EMC a–c and three typical images of data sets obtained in the electrolyte EC/EMC + VC d–f. For easy comparison between the Figures each data set is assigned to a coloured frame that remains identical throughout the manuscript. Importantly, it is observed that the topography of the underlying lithium surface and SEI layer that forms immediately upon contact with the electrolyte is very heterogeneous. Figure 2a shows a distinct crack or step edge in the foil, while in Figs. 2b and 2c a rather smooth surface is probed, exhibiting smaller particles on top. Figure 2d displays a terrace structure on the surface and deep ridges in between. In Figs. 2e and 2f, the surface is covered with few large particles in the micrometre range and several medium sized particles. Furthermore, comparing the topgraphy obtained in the EC/EMC electrolyte (Figs. 2a–2c) with that obtained in EC/EMC with added VC (Figs. 2d–2f), it becomes apparent that VC affects the observed topography significantly. For the EC/EMC electrolyte, the surface is covered by many small particles in a size of approximately 30–100 nm with rather sharp edges. In EC/EMC + VC electrolyte, however, the surface is covered by comparatively larger particles that appear more round-shaped.

Stiffness images were obtained after various immersion times to study the temporal evolution of the surface stiffness. Figure 3

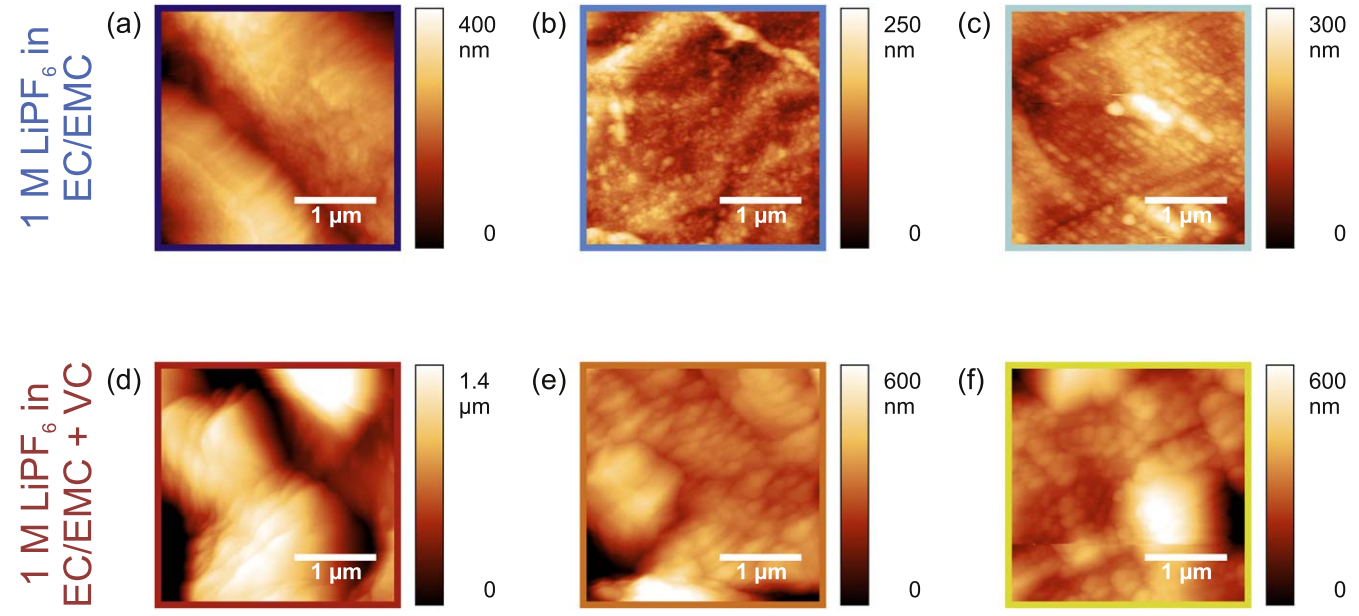

Figure 2. Topography of SEI after immersion EC/EMC electrolyte (a 170 min, b 320 min, c 160 min) and EC/EMC+VC (d 170 min, e 350 min, f 180 min). The coloured frames refer to the colours of the corresponding data sets in Figs. 3 to 6.

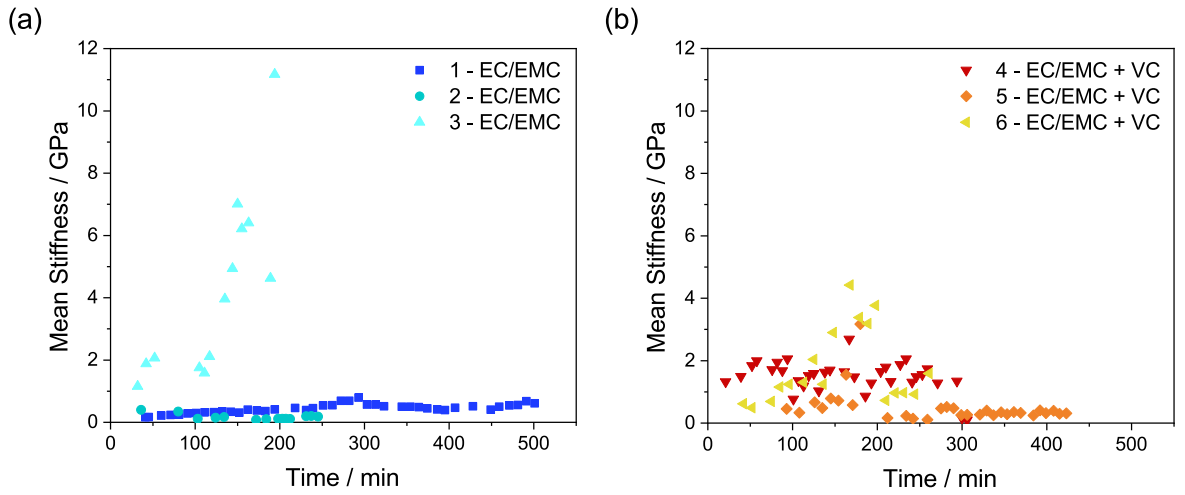

Figure 3. Evolution of mean stiffness with respect to immersion time. a Lithium foil immersed in EC/EMC. b Lithium foil immersed in EC/EMC + VC. Differently coloured data points refer to different data sets (different date, different piece of lithium foil).

illustrates the temporal evolution of the mean stiffness of the SEI. Figure 3a illustrates the mean stiffness of the SEI in EC/EMC electrolyte, Fig. 3b displays the mean stiffness of the SEI in EC/EMC electrolyte with 5 wt% added VC. Please note, in both figures. the mean stiffness values at 0 min represent the pristine Li surface under argon atmosphere before addition of electrolyte. For the EC/EMC electrolyte, the mean stiffness of the SEI is in the range of 0–1 GPa and remains rather constant over time with only slight variations. The only exception is data set 3 (light blue triangles) where the mean stiffness rises significantly after 100 min and reaches up to 11.2 GPa. For the electrolyte with added VC, the mean stiffness of the SEI is overall rather constant as well. However, the distribution appears more heterogeneous in a range of 0–4 GPa. At about 150–200 min, a rise of the mean stiffness can be observed, which is most prominent for data set 6 (yellow triangles). In contrast to the EC/EMC electrolyte shown in Fig. 3a, the mean stiffness drops again after this rise.

Overall, the mean stiffness displays a rather heterogeneous behavior which manifests slightly differently for both electrolytes.

To analyze this heterogeneous behavior further, a closer look is taken at the individual stiffness maps. Figures 4a and 4d show the stiffness maps of the SEI on lithium metal immersed in EC/EMC electrolyte after an immersion time of 100 min a and 300 min d. The respective mean stiffness increases from 300 MPa to 570 MPa, as indicated by the overall brighter color in Fig. 4d. However, if several species with differing stiffness are present on the surface, the mean stiffness calculated from the entire AFM image might not represent the situation well. To account for this, Figs. 4b and 4e show the corresponding histograms of the stiffness maps. The histograms have a bin width of 20 MPa and can be fitted by several Gaussians. The coloured lines in Fig. 4b show the individual Gaussians, while the black line shows the cumulation of these individual Gaussians. For the case of 100 min after immersion, the histogram can be fitted by four individual Gaussians, with individual mean peak stiffnesses of 40 MPa, 161 MPa, 317 MPa and 319 MPa for the red, blue, green and purple line, respectively.

The histogram shown in Fig. 4e corresponding to the stiffness map in d, i.e. after 300 min of immersion, shows a significantly

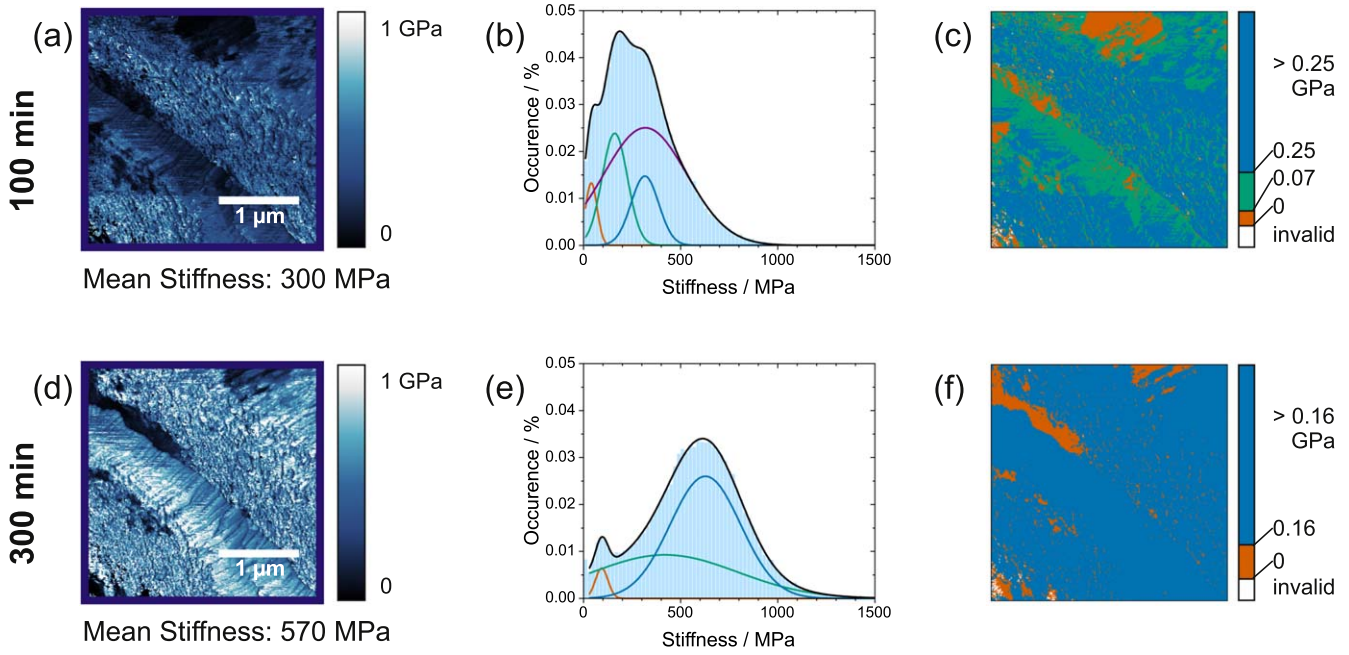

Figure 4. Stiffness maps a, d and respective histograms b, e of lithium foil in EC/EMC after 100 min a–c and 300 min d–f. c, f display the stiffness map color-coded according to the Gaussians that were fit to the histograms b, e. The separation between color blocks corresponds to the intersection of the Gaussians in b, e.

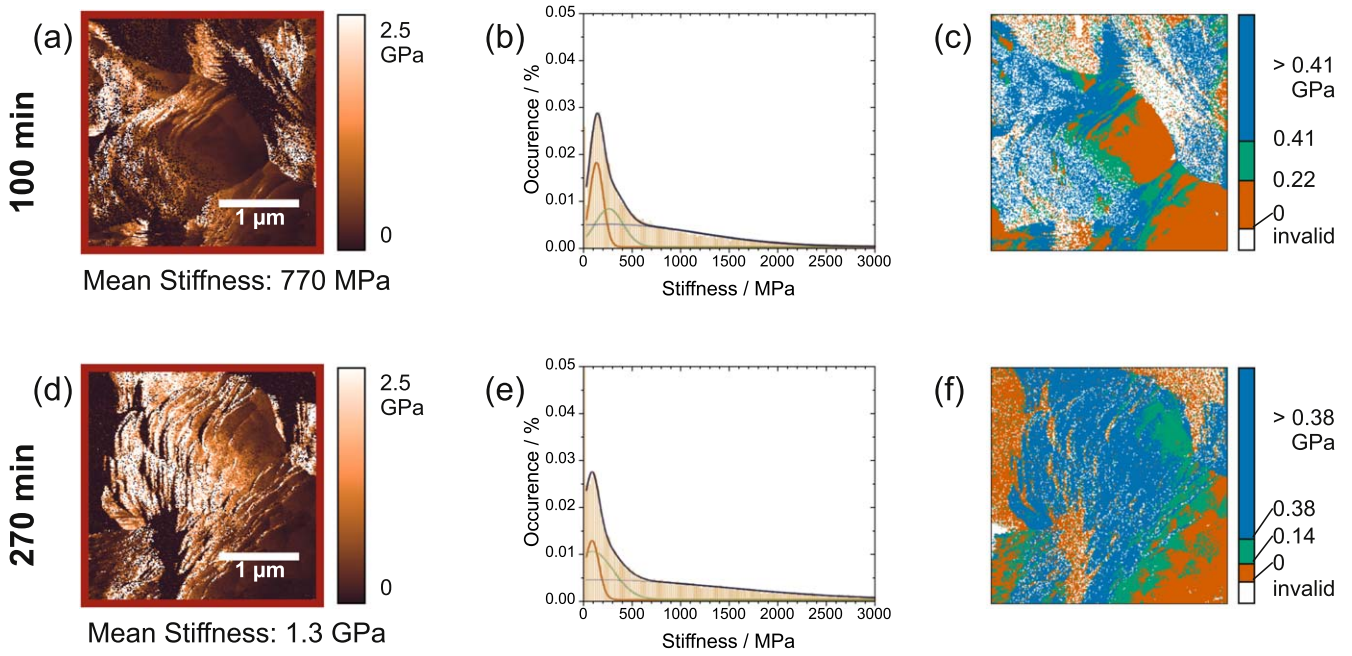

Figure 5. Stiffness maps a, d and respective histograms b, e of lithium foil in EC/EMC+VC after 100 min a–c and 270 min d–f. c, f display the stiffness map color-coded according to the Gaussians that were fit to the histograms b, e. The separation between color blocks corresponds to the intersection of the Gaussians in b, e. White color refers to data points for which no meaningful stiffness values could be calculated from the respective force distance curves.

different distribution. Here, two main peaks can be identified, one of these representing a rather high stiffness around 600 MPa while there is also a smaller second peak at lower stiffnesses around 100 MPa. This clearly demonstrates that the stiffness distribution changes over time.

To illustrate this in more detail, Figs. 4c and 4f show the respective stiffness maps from Figs. 4a and 4d with a color scheme that reflects the peak positions. This representation demonstrates that in Fig. 4c, three main areas displaying a medium (green) or low (red) stiffness between 0 and 250 MPa are present. One region is located at the top right of the image, another area crosses the image from the top left to the bottom right corner. The third area with a low stiffness is located at the bottom left corner of the image. In Fig. 4f, reduced stiffness is observed in these locations as well, but in much smaller areas compared to Fig. 4c.

Similarly to Figs. 4, 5 depicts the stiffness and its histograms for the electrolyte with added VC. Figures 5a and d show the stiffness maps after 100 and 270 min, respectively. The mean stiffness increases from 770 MPa to 1.3 GPa. The corresponding histograms of the stiffness maps, displayed in Figs. 5b and 5d, were approximated by three Gaussians. To further illustrate the stiffness distribution on the surface, the intersections of the Gaussian curves were determined. For the histogram after 100 min (Fig. 5b), the Gaussians intersect at 220 MPa (red and green) and 410 MPa (green and blue). This is represented graphically in the stiffness map in Fig. 5c with a color scheme that reflects the intersections of the Gaussians. For data points represented in white no meaningful stiffness values could be calculated from the respective force distance curves recorded by the AFM. Figure 5f shows the corresponding stiffness distribution map at 270 min. The intersections of the Gaussians in the histogram (Fig. 5e) are at 140 and 380 MPa.

To further analyze the temporal evolution of surface stiffness, a second kind of representation is chosen in the form of stiffness histograms over time. This representation provides more information than the mean stiffness over time (Fig. 3) allowing a more direct comparison of several data sets.

Figure 6a shows the temporal evolution of the stiffness histograms for the EC/EMC electrolyte, Fig. 6b for the EC/EMC + VC electrolyte. Only histograms of images with equal lateral dimensions are shown. As the stiffness depends strongly on the depicted area, thermal drift between AFM images may lead to unwanted effects in evaluation of stiffness data. To minimize this effect, for each electrolyte a data set was chosen where the topographic images of the respective data set show minimal drift of the depicted area. Typical images of the topography at the beginning, middle and end of the same data sets as discussed before are highlighted in Fig. 7.

The temporal evolution in Fig. 6a shows a shift of the main peak toward higher stiffness values throughout time. At first, the position of the main peak shifts slightly toward higher stiffness values. Between 100 and 200 min, its position stays mostly constant while the peak broadens. Afterwards, the position of the main peak shifts to higher stiffness values and reaches a maximum at about 250–300 min, before shifting to lower stiffness values until about 400 min and increasing again afterwards. All throughout, there still is a peak present with reduced intensity at a stiffness of about 100 MPa. This indicates that a species with increased stiffness forms on the surface but nevertheless, a species with lower stiffness remains present the entire time.

In Fig. 6b, the stiffness histograms are displayed for the electrolyte with added VC. Here, the distribution is rather broadly distributed, mostly between 0 and 400 MPa, with individual peaks around 100 MPa. The overall form of the distribution is more heterogeneous than in Fig. 6a and does not necessarily follow a Gaussian form. Over time, there are small flucutations in peak intensities and positions, but overall the range of stiffness remains unchanged.

Discussion

For the interpretation of the stiffness data, the experimental conditions have to be taken into account. To avoid significant interaction between the tip and the surface throughout the measurement period, a moderate setpoint of 50–100 nN (without VC), 150–200 nN (with VC) was chosen. This resulted in an indentation depth in the order of 5–20 nm. Xu et al. reported a SEI layer thickness of 18 to 20 nm in similar electrolytes, measured by TEM in dry conditions. As Zhang et al. reported, the SEI layer swells in electrolyte environment with respect to a dry layer.[31] Therefore, the SEI layer is expected to be thicker than 20 nm in electrolyte. Hence,

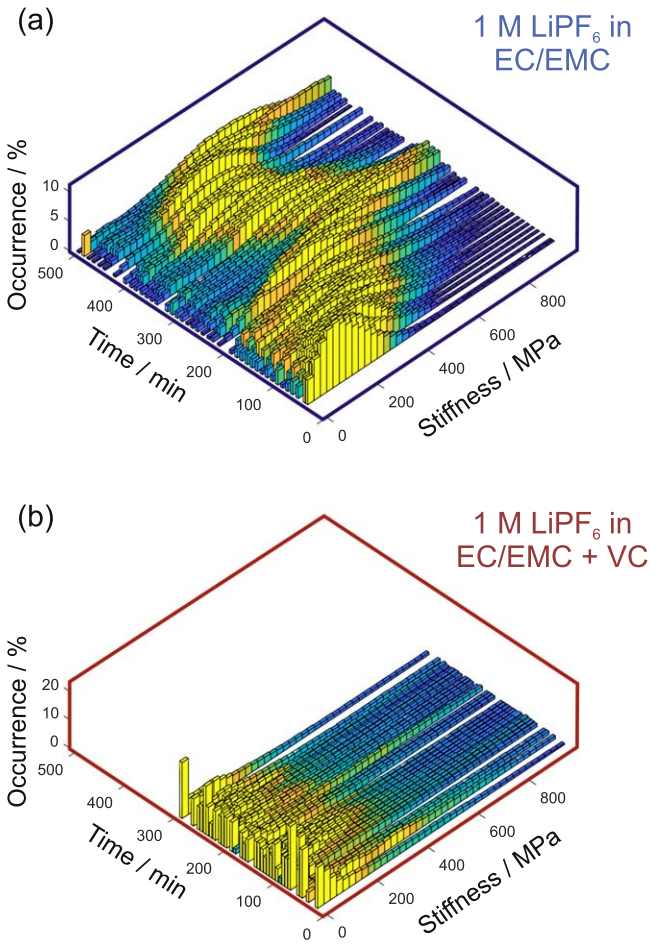

Figure 6. Temporal evolution of stiffness histograms of SEI on lithium metal in electrolyte a EC/EMC and b EC/EMC + VC.

it is assumed that only the topmost layer of the interphase was probed in the presented in situ experiments. Thus, the thickness of the SEI layer does not influence the accuracy of the DMT model used in the presented work.

Considering the morphology of the SEI layer, a clear influence of the VC additive is visible. The larger and more round-shaped particles that form in presence of VC possibly indicate a very soft layer covering the particles. Alternatively, a "wobbly" layer underneath the particles is also possible. This is in accordance with the organic domains observed by Xu et al.[21]

Concerning the stiffness, no clear influence of VC is visible in the temporal evolution of the mean stiffness. Taking a closer look at the stiffness in the form of the temporal evolution of histograms, however, a clear influence of VC can be identified. Comparing the data sets in Figs. 6a and 6b, it is observed that the vinylene carbonate seems to have a stabilising effect on the mechanical properties in the sense that there are less variations. The stiffness distribution is more homogeneous throughout time compared to the electrolyte without VC. Furthermore, the stiffness distribution exhibits a high number of larger peaks at low stiffness values. This can be attributed to the organic domains that form when VC is reduced. Additional organic species are also present from the reduction of EC and EMC. The main SEI component resulting from the reduction of EC is lithium ethylene dicarbonate (LEDC),[32] other components that are present in much lower fractions are lithium ethylene monocarbonate (LEMC) and dilithium ethylene monocarbonate (DLEMC).[33] Kamikawa et al. calculated elastic moduli for poly(VC), the polymer of VC, in a range of 1.76–3.82 GPa.[34] This does not relate to the peaks in the histograms in Figs. 5b and 5d at about 200 MPa. However, this is in accordance with the rather broadly distributed stiffness up to 3 GPa that is visible in these histograms. As the stiffness of polymers depends on the degree of cross-linking,[35] this also explains the broad distribution as most probably a wide variety of degrees of cross-linking is present. For the electrolyte without VC, there is a (small) peak present at low stiffnesses (below 200 MPa), possibly reflecting the organic components formed from the reduction of EC and EMC. The main peak of the histogram shifts throughout time. This shows that through continuous reaction the surface composition changes locally.

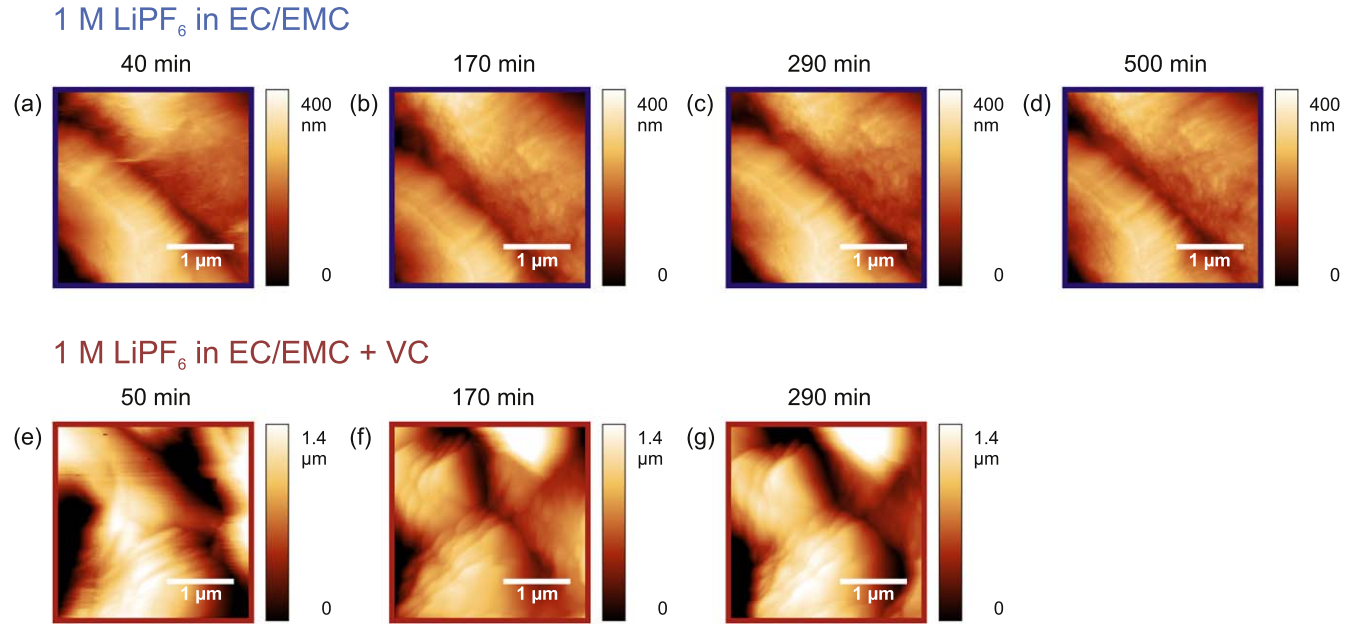

Figure 7. Topography of the SEI throughout the measurement period in electrolytes a–d EC/EMC and e–g EC/EMC + VC. The chosen times depict the topography at the beginning, middle and end of the respective data set. This corresponds to 40 min, 170 min, 290 min and 500 min for the EC/EMC electrolyte and 50 min, 170 min and 290 min for the EC/EMC + VC electrolyte.

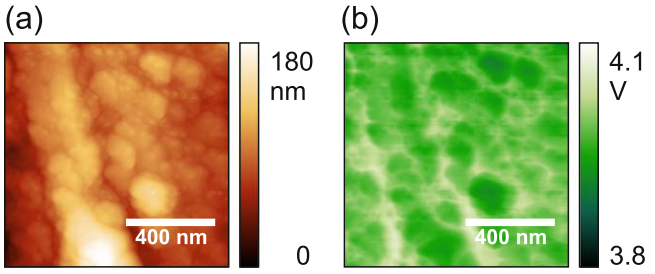

Figure 8. a Topography and b surface potential of lithium foil.

Looking at the individual histograms, their form can be approximated by several Gaussians. This demonstrates that there are several species with differing stiffness present on the surface at the same time. However, it is not reasonable to use this approach to determine the exact number of species with certainty, as there might be species with similar stiffness. From the range of stiffness values present, the lower values are expected to belong to organic species. However, it is not possible to identify all of the individual species of the SEI by their stiffness at this time.

As the SEI forms at the interface between lithium metal and electrolyte, it is noteworthy to take a look at the lithium metal surface as well. To proof a possible intrinsic heterogeneity of lithium foil, the surface potential of the surface has been probed by Kelvin Probe Force Microscopy (KPFM). Figure 8 shows a KPFM image of lithium foil in dry conditions without addition of any electrolyte. Figure 8a displays the topography and Fig. 8b depicts the surface potential of a piece of lithium foil. Here, variations in the surface potential are observed, indicating a different chemical nature of the species at the surface.

The heterogeneity of the lithium foil surface is likely caused by a native layer of reaction products on the surface due to the high reactivity of lithium. Such a layer is typically present on any piece of lithium foil that has not been freshly cleaned since it forms immediately with any surrounding reactants. This causes a heterogeneity that significantly influences further measurements. Ismail et al. determined for lithium foil from the same supplier that the lithium metal is covered by a native film consisting of an outer layer of Li_2CO_3/LiOH and an inner layer of Li_2O.[36] A carbonate layer is typically caused by a passivation treatment of the lithium surface with CO_2.[37] Otto et al. observed a similar composition of the surface film.[38] They also showed that while these surface films are mainly homogeneous with local contaminants, storage and transport conditions lead to inhomogeneity of lithium samples. Looking at the stiffness values of the lithium metal surface studied in this work, hardly any of the observed values fit to the expected Young's modulus of lithium of 4.9 GPa[39] to 7.8 GPa.[40] A much better fit is the Young's modulus of lithium carbonate which was predicted as 36.2 GPa for amorphous lithium carbonate and 54.8 GPa for crystalline lithium carbonate by Shin et al.[22] This confirms the presence of a lithium carbonate layer atop the lithium metal. For comparison, a mean stiffness of 2.8 GPa is determined on lithium foil where the surface layer has been removed. This value is a good fit to the aforementioned values of the Young's modulus of lithium metal.

Conclusions

The influence of VC on the mechanical properties of the SEI layer on lithium metal was studied for the first six hours of SEI formation. The SEI was formed by immersion of lithium in electrolyte without application of a potential. It was demonstrated that the VC additive stabilises the SEI surface. For electrolyte with VC, the stiffness of the SEI layer is between 0 and 300 MPa. For the electrolyte without VC, the stiffness varies between 0 and 1 GPa. Furthermore, it was shown that the SEI layer consists of several species with different stiffness and that the composition changes over time. The key effect of the VC additive is its influence on the homogeneity of the surface layer. Moreover, the presence of VC changes the morphology of the surface, leading to larger and more round-shaped particles.

Considering the dry lithium metal surface, its heterogeneity was demonstrated. The stiffness obtained from the lithium surface indicates a surface layer containing Li_2CO_3.

Acknowledgments

The authors would like to acknowledge the financial support from the Helmholtz Association and the German Federal Ministry of Education and Research (BMBF) within the LILLINT project (13XP0225C). We thank L.G.J. de Haart and R.-A. Eichel for continuous support and fruitful discussions.

ORCID

Beatrice Wolff https://orcid.org/0000-0002-3252-5464
Florian Hausen https://orcid.org/0000-0001-5712-6761

References

1. J. Liu et al., *Nat. Energy*, **4**, 180 (2019).
2. W. Xu, J. Wang, F. Ding, X. Chen, E. Nasybulin, Y. Zhang, and J. G. Zhang, *Energy Environ. Sci.*, **7**, 513 (2014).
3. D. Lin, Y. Liu, and Y. Cui, *Nat. Nanotechnol.*, **12**, 194 (2017).
4. J. M. Tarascon and M. Armand, *Nature*, **414**, 359 (2001).
5. X. He et al., *Nature Reviews Materials*, **6**, 1036 (2021).
6. M. S. Whittingham, *Proc. IEEE*, **100**, 1518 (2012).
7. E. Peled, *J. Electrochem. Soc.*, **126**, 2047 (1979).
8. B. Horstmann et al., *Energy Environ. Sci.*, **14**, 5289 (2021).
9. S. J. An, J. Li, C. Daniel, D. Mohanty, S. Nagpure, and D. L. Wood, *Carbon*, **105**, 52 (2016).
10. S. S. Zhang, *Electrochem. Solid-State Lett.*, **162**, 1379 (2006).
11. D. Aurbach, K. Gamolsky, B. Markovsky, Y. Gofer, M. Schmidt, and U. Heider, *Electrochimica Acta*, **47**, 1423 (2002).
12. K. Xu, *Chem. Rev.*, **114**, 11503 (2014).
13. O. Matsuoka et al., *Electrochem. Solid-State Lett.*, **108**, 128 (2002).
14. H. Ota, Y. Sakata, A. Inoue, and S. Yamaguchi, *J. Electrochem. Soc.*, **151**, A1659 (2004).
15. G. Zampardi, F. La Mantia, and W. Schuhmann, *Electrochem. Commun.*, **58**, 1 (2015).
16. L. Lin, K. Yang, H. Chen, and F. Pan, *Functional Materials Letters*, **10**, 1750052 (2017).
17. S. Grugeon, P. Jankowski, D. Cailleu, C. Forestier, L. Sannier, M. Armand, P. Johansson, and S. Laruelle, *J. Power Sources*, **427**, 77 (2019).
18. G. Zheng et al., *Energy Storage Materials*, **29**, 377 (2020).
19. H. Ota, Y. Sakata, X. Wang, J. Sasahara, and E. Yasukawa, *J. Electrochem. Soc.*, **151**, A437 (2004).
20. F. M. Weber, I. Kohlhaas, and E. Figgemeier, *J. Electrochem. Soc.*, **167**, 140523 (2020).
21. Y. Xu, H. Wu, Y. He, Q. Chen, J. G. Zhang, W. Xu, and C. Wang, *Nano Lett.*, **20**, 418 (2020).
22. H. Shin, J. Park, S. Han, A. M. Sastry, and W. Lu, *Electrochem. Solid-State Lett.*, **277**, 169 (2015).
23. X. Shen, R. Zhang, X. Chen, X. B. Cheng, X. Li, and Q. Zhang, *Adv. Energy Mater.*, **10**, 1903645 (2020).
24. D. Aurbach, *J. Electrochem. Soc.*, **143**, 3525 (1996).
25. Y. S. Cohen, Y. Cohen, and D. Aurbach, *J. Phys. Chem.* , B **104**, 12282 (2000).
26. Z. Zhang, K. Smith, R. Jervis, P. R. Shearing, T. S. Miller, and D. J. L. Brett, *ACS Applied Materials & Interfaces*, **12**, 35132 (2020).
27. S. Benning, C. Chen, R. A. Eichel, P. H. L. Notten, and F. Hausen, *ACS Appl. Energy Mater.*, **2**, 6761 (2019).
28. C. Chen et al., *Nat. Commun.*, **11**, 3283 (2020).
29. Quantitative Mechanical Property Mapping at the Nanoscale with PeakForce QNM, Application Note #128, Bruker.
30. B. Derjaguin, V. Muller, and Y. Toporov, *J. Colloid Interface Sci.*, **53**, 314 (1975).
31. Z. Zhang et al., *Sci.*, **375**, 66 (2022).
32. G. V. Zhuang, K. Xu, H. Yang, T. R. Jow, and P. N. Ross, *J. Phys. Chem.* , B **109**, 17567 (2005).
33. E. W. C. Spotte-Smith, R. L. Kam, D. Barter, X. Xie, T. Hou, S. Dwaraknath, S. M. Blau, and K. A. Persson, *ACS Energy Lett.*, **7**, 1446 (2022).
34. Y. Kamikawa, K. Amezawa, and K. Terada, *J. Phys. Chem. C*, **124**, 19937 (2020).
35. R. F. Landel and L. E. Nielsen, *Mechanical Properties of Polymers and Composites* (New York)(Marcel Dekker) (1993).
36. I. Ismail, A. Noda, A. Nishimoto, and M. Watanabe, *Electrochimica Acta*, **46**, 1595 (2001).
37. T. Fujieda, N. Yamamoto, K. Saito, T. Ishibashi, M. Honjo, S. Koike, N. Wakabayashi, and S. Higuchi, *Electrochem. Solid-State Lett.*, **52**, 197 (1994).
38. S. K. Otto, Y. Moryson, T. Krauskopf, K. Peppler, J. Sann, J. Janek, and A. Henss, *Chem. Mater.*, **33**, 859 (2021).
39. R. P. Schultz, Smithells metals reference book, (Elsevier Butterworth-Heinemann, Amsterdam) (2004), https://www.osti.gov/biblio/804180.
40. A. Masias, N. Felten, R. Garcia-Mendez, J. Wolfenstine, and J. Sakamoto, *J. Mater. Sci.*, **54**, 2585 (2019).